DTU Wind and Energy Systems

Development of a coupling framework for wind turbine aeroelastic steady-state calculations

Julio Vázquez Martínez-Lozano

DTU Wind-M-0864
July 2024

Author:
Julio Vázquez Martínez-Lozano

Title:
Development of a coupling framework for wind turbine aeroelastic steady-state calculations

DTU Wind-M-0864
July 2024

ECTS: 30

Education: Master of Science

Supervisor(s):

Taeseong Kim
Ang Li
DTU Wind & Energy Systems

Mehmet Ozan Gözcü
ØRSTED

Remarks:
This report is submitted as partial fulfillment of the requirements for graduation in the above education at the Technical University of Denmark.

DTU Wind & Energy Systems is a department of the Technical University of Denmark with a unique integration of research, education, innovation and public/private sector consulting in the field of wind energy. Our activities develop new opportunities and technology for the global and Danish exploitation of wind energy. Research focuses on key technical-scientific fields, which are central for the development, innovation and use of wind energy and provides the basis for advanced education at the education.

Technical University of Denmark
Department of Wind and Energy Systems
Frederiksborgvej 399
4000 Roskilde
Denmark
www.wind.dtu.dk

Approval

Julio Vázquez Martínez-Lozano - s222926

.....

Signature

.....

Date

Abstract

The wind energy industry relies on computer-aid engineering tools to design and optimize wind turbines. Modern wind turbines have larger and relatively more flexible blades, that can challenge passed modeling assumptions. Consequently, new methods are being developed to better understand and model the behaviour of the rotors. The aeroelastic modeling of wind turbines requires the use of both an aerodynamic model and a structural model, which address the complexities of each discipline separately. These models must then be coupled to arrive to a unified solution of the system. Since coupling to existing wind turbine models can sometimes be challenging, it is interesting to do it in a more modular way..

In this project, two open-source models are coupled to create an aeroelastic steady-state model for wind turbines, using a framework to increase the modularity of the code components. The Blade Elements Vortex Cylinder (BEVC) model is used for aerodynamics and the co-rotational based structural model, CoRot, is used for structural dynamics. The method used for the coupling is the fixed-point iteration method.

After implementation, the model is validate against HAWC2, the state-of-the-art DTU aeroelastic model, across various operational conditions using the IEA 15 MW reference wind turbine. This validation demonstrates the accuracy and reliability of the resulting model. Additionally, the convergence behaviour of the coupling is explored for different discretization levels of the wind turbine's blades. The results confirm that the model converges at a linear rate, as expected with the coupling methods used, requiring fewer than ten iterations. The convergence study also allows for the comparison of discretization levels based on the minimum achieved error, which shows good results even for low discretization levels.

Acknowledgements

I would like to express my gratitude to my supervisors for their advice and guidance during our meetings and our email exchanges. Special thanks to Kim Taeseong for all the weekly meetings, to Ozan Gözcü for his guidance with the structural code and to Ang Li for the help with the aerodynamic code and HAWC2.

As this project marks the end of a beautiful period of my life, I would like to thank all my loved ones for their support. In particular to my mother, *porque sin tu gran labor de madre todos estos años, no habría llegado a donde estoy*.

Contents

1 Introduction

1.1 Background

Wind energy has emerged as a pivotal element in the global shift towards sustainable energy solutions. As nations strive to meet ambitious net zero targets, the role of renewable energy sources, particularly wind power, has become increasingly crucial. The drive for decarbonization, emphasised by international commitments to reduce greenhouse gas emissions, has accelerated the adoption and advancement of wind energy technologies.

One of the most notable trends in the wind energy sector is the rapid growth in the size and capacity of wind turbines. Since the advent of the first industrial turbines in the late 1970s, there has been a dramatic increase in both rotor diameter and power output. Modern wind turbines now approach capacities of 15 MW, with rotor diameters exceeding 200 meters. This increase in size is not merely a feat of engineering; it translates to significant economic and operational benefits, including reduced maintenance costs and enhanced energy capture efficiency.

Technological advancements have also focused on improving the flexibility and performance of wind turbine blades. The development of larger, more efficient blades requires sophisticated design and materials engineering to handle the complex aerodynamic and gravitational loads. Flexible blades, capable of adjusting to varying wind conditions, enhance the overall efficiency and durability of wind turbines, making them more adaptable to diverse environments.

The impact of these innovations extends beyond mere technological progress. The expansion of wind energy capacity is a critical component of global energy strategies aimed at achieving net zero emissions. According to forecasts by the International Energy Agency (IEA), substantial increases in renewable energy capacity are essential to meet the targets set for 2050. Achieving these goals will require not only continued policy support and investment but also significant advancements in wind turbine technology [1, 2].

1.2 Literature review and motivation

Computer-aided engineering tools

For the design of wind turbines, the use of computer-aided engineering (CAE) is very relevant. These computer tools help assist the design and evaluation of the wind turbines, taking into account the relevant physical phenomena to analyse performance, loading and stability [3, 4].

These tools join together a series of physics models that model the different phenomena that affects a wind turbine and how it reacts, see figure 1.1. The models cover different

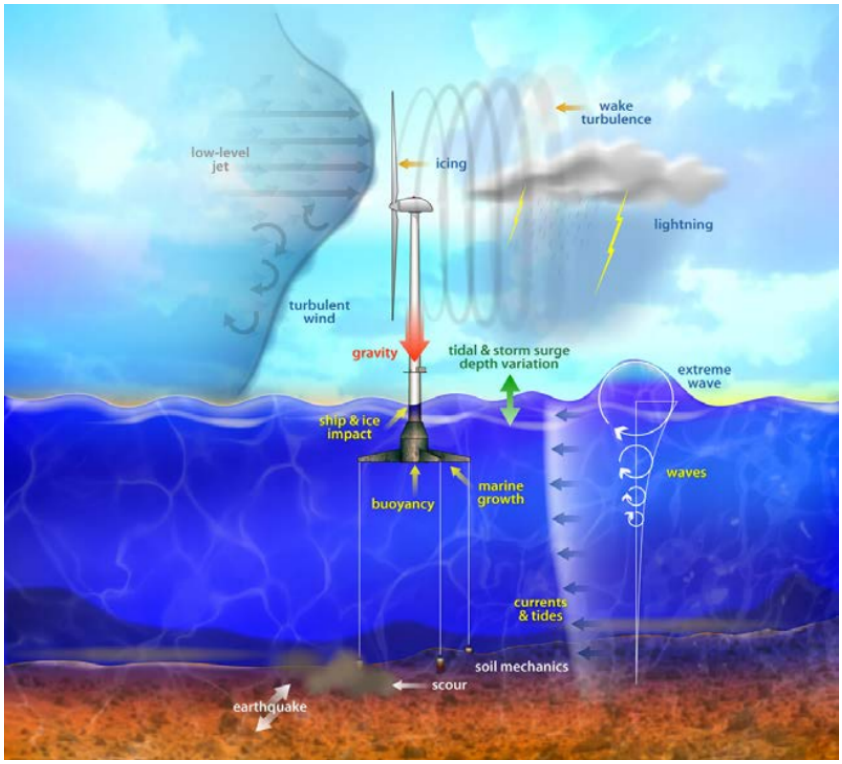

Figure 1.1: Different physical phenomena that affects a floating wind turbine [4].

disciplines such as aerodynamics, hydrodynamics, structural dynamics, electrical and control. Each discipline can have different models of different fidelities and assumptions.

The CAE tools cannot always solve the fundamental laws of physics, since it would be slow and costly. Instead, they rely on engineered models that are derived from the fundamental laws of physics, but apply significant and reasonable assumptions.

The CAE tools for wind turbines are also called aeroelastic or aero-servo-elastic tools, meaning that these tools can model the interactions between the aerodynamic loads, the inertial loads, the elastic forces and the actuation of the feedback control system of wind turbines.

Aeroelasticity

Aeroelasticity is the discipline concerned with the interaction between aerodynamic forces, elastic forces and dynamic forces, see figure 1.2. These interactions are strong in wind turbines, helicopters and airplanes, making this discipline important in these fields [5].

In such structures, aerodynamic forces depend on the relative velocities of the air flowing around the structure. These structures are flexible, meaning that the different loads acting in the structure can bend them, which in turn affects the aerodynamic forces.

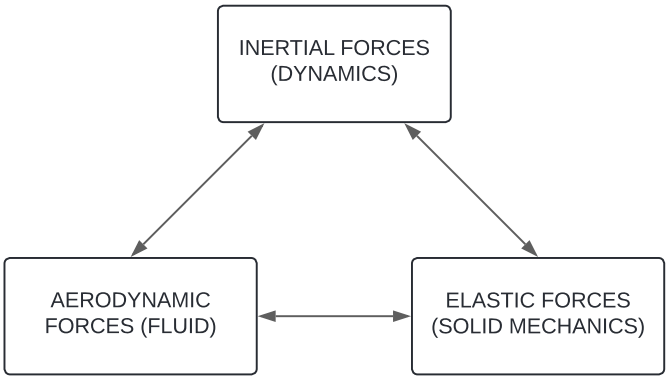

Figure 1.2: Aeroelasticity is the discipline concerned with the interaction between aerodynamic forces, elastic forces and dynamic forces [6].

For this reason, in the wind industry most of the CAE tools used, perform aeroelastic simulations. Some of these models analyze the dynamic response in the time domain or in steady-state.

Steady-state of a wind turbine

The steady-state analysis of a wind turbine involves employing simplifying assumptions to eliminate loads that vary relative to the rotor's rotation, thereby ensuring that all blades are experiencing the same loads. By removing these time-varying loads, the state of the wind turbine becomes time-independent, or steady-state. This is achieved by assuming a uniform wind inflow in the rotor, neglecting the effects of gravity and presuming identical deflections and pitch angles for all blades [7].

While these assumptions may appear unrealistic, the resultant models provide accurate and reliable results that are valuable in numerous applications. These models are computationally efficient and fast, making them ideal for evaluating wind turbine rotor performance, generating precise power and thrust curves. Furthermore, they are essential in the rotor design process, from preliminary design phases, where key parameters are determined, to detailed optimization stages. This efficiency is facilitated by the capacity to compute performance gradients with respect to design variables.

Current aeroelastic tools

There are different state-of-the-art models for wind turbines that are widely used in the industry and in research, these include: HAWC2, Bladed, OpenFAST and QBlade [8] .

All these models use for aerodynamics the blade element momentum (BEM) theory with some corrections to account for stall and other effects in the rotor. For the structure, they use flexible multibody formulations with flexible elements modelled as beams. They all have non-linear blade deformations, although they have different formulations

to account for that.

In this project the HAWC2 model is going to be used as a benchmark. This model was developed at Risø National Laboratory for Sustainable Energy and it is widely used in industry and research of wind turbines. In section 3.2.1 there are more details about how is was used.

Modularity

Aeroelastic tools consist of various models, each representing a different physical phenomenon they aim to simulate. These models are often conceived and developed using specific fields of knowledge. In commercial tools, wind turbine CAE tools can include different models for rotor aerodynamics, the control loop, structural dynamics and foundations hydrodynamics (for offshore wind turbines), as illustrated in figure 1.3. Each of these models comprises a set of equations that need to be solved for a given configuration and state of the system.

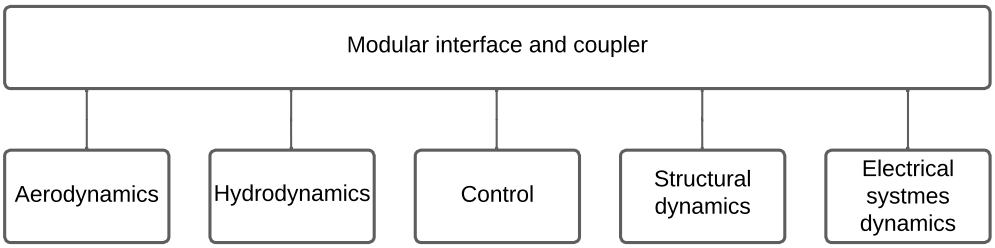

Figure 1.3: Illustration of the modularity of a modern CAE tool for wind turbines. Inspired by [4]

The primary advantage of modularity is that it allows the models to be interchanged without affecting the other modules. This flexibility is crucial for benchmarking and research, as it enables the testing and comparison of different models. Additionally, different applications require different levels of fidelity, which can be achieved with different models. Over the years there has been an effort to integrate this modularity in industry tools such as FAST [4, 3].

Modular frameworks

To achieve this modularity in the implementation of the tools, frameworks are an essential concept to make use of.

In the broadest and most precise sense, “a framework is a reusable design of a system that is represented by the set of abstract classes and the way their instances interact” [9]. The idea is that the “components” that these abstract classes represent, free the software developer or engineer of knowing the underlying implementation. In other words, it works as the skeleton of the tool that can be customized for the needs.

This way of developing the code makes modularity part of the way it was coded. In this specific application, the framework aims to achieve the following objectives:

- Compartmentalize the modules, so that the implementation of a module does not affect the rest of them.
- Couple the modules, the framework has to be able to couple the modules to get a solution.

New models

There are still new methodologies to model the different phenomena in a wind turbine and new models are continuously being researched and developed.

However, using these new methodologies in the current models can be complicated because of how these need to be implemented in the code. The lack of flexibility can lead to a lot of problems and make worse the efforts to develop the models.

In this project, two new open-source models are going to be used: a structural model with a co-rotational formulation [10] and a aerodynamic code based on the Vortex-Cylinder model [11].

1.3 Project objective

The objective of this project is to develop a coupling framework for wind turbine aeroelastic steady-state calculations. This will involve integrating two existing open-source codes: a vortex cylinder based aerodynamic model code and a co-rotational based beam model code developed by DTU Wind. The resultant tool aims to be a flexible and modular framework that can facilitate the integration of additional models in the future.

To ensure the tools reliability and accuracy, it will be validated against the state-of-the-art code HAWC2. Additionally, the project will assess the effects of different discretization levels through a convergence study, further establishing the tool's performance and robustness.

2 Implementation

This chapter presents a detailed overview of the implementation of the aeroelastic steady-state model. It begins with an overview of the wind turbine definition used in the engineering tools. Then, there is an examination of the model parameters, inputs and outputs. This is followed by an explanation of how they are coupled in steady-state and an explanation of the framework that was developed.

2.1 Wind turbine definition

In this project, a horizontal wind turbine rotor is going to be modelled. The two solvers employ the conventions established by HAWC2 for defining the structure inertial, elastic and aerodynamic properties.

2.1.1 Coordinate systems

A wind turbine consists of several bodies, each with different structural and aerodynamic properties. In this project, only the rotor is modeled, which includes a number of blades held by the hub. The blades are free to rotate on the hub, allowing the blades to pitch. Additionally, the hub is connected to the shaft, which rotates at a constant speed, Ω.

The different bodies have their own frames of reference. The most relevant frames of reference for this model are:

- Inertial frame, I. This basis is oriented with the y-axis in the wind direction and the z-axis pointing upwards.
- Rotor frame, R. This frame of reference is fixed to the rotor and rotates with it. It has the y-axis oriented in the wind direction and the z-axis extends radially from the rotor centre. Each of the blades have their own rotor frame of reference.
- Blade's root frame, BR. This frame is fixed to the root of the blade, located at the hub radius distance from the rotor center. Because it is fixed to the blade, it rotates with both the rotor and the pitch of the blade.
- Blade element frame, E. Each of the blade elements have their own axis with the x-axis oriented towards the leading edge, the y-axis in the flap direction and the z-axis oriented forwards in the blade.

The blades that can be simulate in this model have no tilt angle and no cone angle. The tilt angle is defined as the angle between the normal of the rotor plane and the horizontal plane. The cone angle is defined as the angle between the $z_{_{BR}}$-axis and the rotor plane.

2.1.2 Blade properties definition

Both models have a blade definition based on the HAWC2 conventions. To define the rotor, it is necessary to know the blade's geometry, its aerodynamic layout and airfoil aerodynamic properties, and the blade's structural properties.

Geometry

The blade is defined along the half-chord centres of its airfoils, the centre line. Along this curve the different aerodynamic layouts and structural properties are defined (see figure 2.1).

In HAWC2, this definition is provided in the HTC file using the parameters shown in table 2.1. Here the location of each point in the blade's root coordinate system and the blade twist are defined. The latter is used to orient the different element frames of reference for other properties, see figure 2.2.

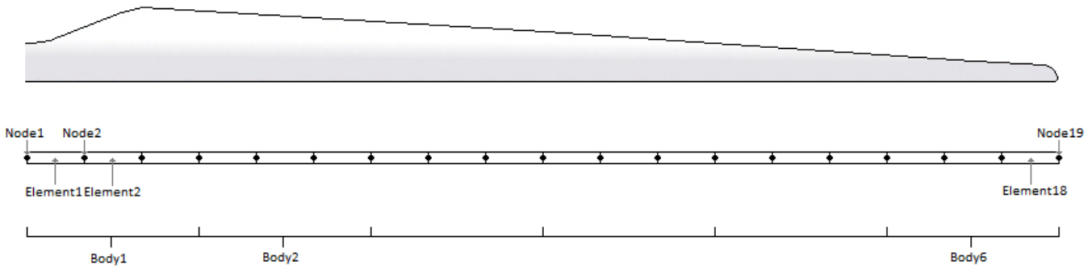

Figure 2.1: discretization of the blade in HAWC2 [12]. The blade has elements that go in between nodes.

Parameter	Unit	Explanation
N	-	Half-chord node number, from one and up.
X, Y, Z	m	Location of the half-chord nodes in the blade root coordinate system.
$\theta_{z,\,twist}$	deg	Angle between the x_{c2}-axis and the X_{c2}-plane, defined positive for rotations around the z_{c2}-axis.

Table 2.1: Parameters given to define the half-chord centre line.

Aerodynamic properties

For each of the nodes of the blade there is a different airfoil being used. To define it, it is needed to define the chord length and the thickness ratio of the specific airfoil, figure 2.2a. To get the aerodynamic characteristics of the blades, it is also needed to give the static aerodynamic properties of each of the profiles used. In HAWC2 the AE file and PC file have this information respectively.

Structural properties

The blade's structural properties include its mass distribution and stiffness characteristics. The mass is specified as a distribution along its centres of mass. The stiffness properties of the node can be defined in two formats:

- Isotropic beam (original HAWC2's input). This format assumes the beam is isotropic, meaning its mechanical properties are the same in all directions.

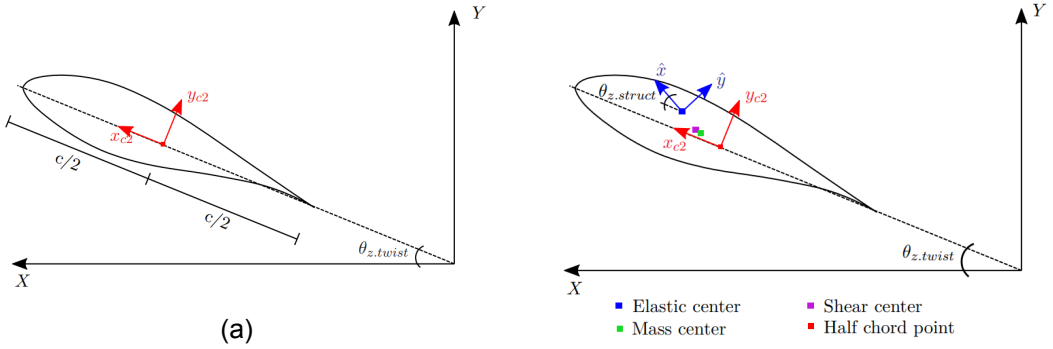

(a) (b)

Figure 2.2: (a) Geometry of an airfoil section. (b) The centre of mass (green), shear centre (purple) and elastic axes (blue) are defined with respects to the half chord axis (red) [13].

- Anisotropic beam. This more complex format assumes the beam is anisotropic, meaning its mechanical properties vary with direction. It uses a fully populated stiffness matrix to capture these variations.

The structural properties are stored in the ST file for HAWC2 inputs. Table 2.2 shows the structural properties that need to be defined depending on the chosen format, as each one has specific parameters.

2.1.3 Operational and wind inflow conditions

For the steady-state case, the wind inflow is required to be the same in the whole rotor. This means that it has to be perpendicular to it and of constant magnitude, which is only achieved with a uniform wind inflow, without any tower shadow model and without any yaw angle.

Placed in this wind, the wind turbine is operated at a constant rotational speed and pitch angles. Given these conditions, the wind turbine will achieve a certain steady-state deflections and loading.

The wind turbine on this model can have a series of parameters that define its operational conditions, shown in 2.3.

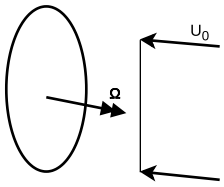

Figure 2.3: The rotor has a uniform wind inflow, U_0, and a constant rotational speed, Ω and pitch angle, θ_p.

2.2 The different models

The steady-state model of the wind turbine rotor is made out of three distinct models: the aerodynamic model, the structural model and the inertial model. The aerodynamic model calculates the aerodynamic loads for a specific operational

Parameter	Symbol	Unit	
Curved length distance	r	m	
Mass per unit length	m	kg/s	
x_{c2}-coordinate from $C_{1/2}$ to mass centre	x_m	m	
y_{c2}-coordinate from $C_{1/2}$ to mass centre	y_m	m	
Structural pitch about z_{c2}	Θ_s	deg	
x_{c2}-coordinate from $C_{1/2}$ to centre of elasticity	x_e	m	
y_{c2}-coordinate from $C_{1/2}$ to centre of elasticity	y_e	m	
Radius of gyration related to elastic centre. Rotation about principal bending x_e	r_{ix}	m	
Radius of gyration related to elastic centre. Rotation about principal bending y_e	r_{iy}	m	
x_{c2}-coordinate from $C_{1/2}$ to shear centre	x_s	m	HAWC2 Input
y_{c2}-coordinate from $C_{1/2}$ to shear centre	y_s	m	
Modulus of elasticity	E	N/m^2	
Area moment of inertia with respect to principal bending x_e	I_x	m^4	
Area moment of inertia with respect to principal bending y_e	I_y	m^4	
Torsional stiffness	K	m^4/rad	
Shear factor for force in principal bending x_e direction	k_x	-	
Shear factor for force in principal bending y_e direction	k_y	-	
Cross sectional stiffness matrix element	K_{ab}	N, Nm or Nm^2	FPM

Table 2.2: Structural data input parameters. There are two ways of setting this data: the HAWC2 input and the fully populated matrix (FPM) case. Some parameters are common to both methods, while others are unique to each.

and wind condition; the structural model determines the deflections of the blades given the loads, and the inertial model adjusts the structural to account for a moving frame of reference.

Each of the models is initialized with the necessary rotor parameters in its specific file format. Furthermore, each model has its own inputs and outputs that need to be communicated to achieve the coupling. This can be challenging, as each model has specific details for these variables, often requiring intermediate transformations (such as changes in shape or frame of reference).

2.2.1 Aerodinamic model: BEVC

The Blade Element Vortex Cylinder (BEVC) model, developed at DTU, is the aerodynamic model used in this project. This code is based on a vortex cylinder model [11] of the rotor and it is fundamentally different from Blade Element Moment (BEM) models, which are the most often used for this application. These models represent an optimal balance between speed and model fidelity for the modelling of wind turbine rotors.

BEM models are based on a number of assumptions regarding the rotor, including the assumption that it is a planar rotor and that there is no interaction between the different stream tubes. As a result, the model is less accurate when the blades are out of plane,

Operational conditions		
Tip-speed ratio	TSR	In its defect, the rotational speed, ω. TSR$= \omega \cdot R/U_0$
Pitch angle	θ_p	The same pitch for all blades.
Wind inflow conditions		
Free wind speed	U_0	Uniform wind inflow.
Air density	ρ	

Table 2.3: Operational and wind inflow conditions parameters.

Variable	**Aerodynamics**	**Structural Dynamics**
Inputs	Turbine displacements	Aerodynamic loads
Outputs	Aerodynamic loads Power and thrust Induction	Displacements Reaction loads
Parameters	Turbine geometry Static airfoil data Undisturbed wind inflow Operational conditions	Turbine geometry Mass/Inertia Stiffness Operational conditions

Table 2.4: Inputs, outputs and parameters of the aerodynamic and structural models.

which can occur with blades that have a large prebend, cone angle or deflections. To address these issues, a number of corrections have been developed for BEM models. Nevertheless, BEVC employs a distinct methodology that entails the construction of the appropriate assumptions to accommodate the out-of-plane effects in aerodynamics. This approach allows for the achievement of more reliable and accurate results with a comparable computational speed.

The BEVC model is implemented in Fortran and is accessible via a Python library, which serves as an interface between the main code and external applications. The code has previously undergone rigorous testing and implementation within HAWC2, resulting in high compatibility with HAWC2's input and output conventions and file formats. Consequently, the implementation within the framework utilises HAWC2 files as input, which facilitates the input process and will also ease comparison against the HAWC2 results.

Initialization

To calculate the rotor loads, the BEVC model requires the rotor geometry, the aerodynamic properties of the airfoil used, and the operational and inflow conditions, as summarized in table 2.4.

As explained in section 2.1, this information can be found in a series of files in a typical HAWC2 input. Due to the HAWC2 input support of this model, the main HAWC2 file, the HTC file, contains all information required, namely the centre line data and the names of the remaining files. It should be noted that only this data is collected from the HTC

file and no other commands are considered, such as wind inflow, HAWC2 commands or other bodies data.

The operational conditions (i.e. rotational speed and pitch angle) and wind inflow conditions are not taken from the HAWC2 input, but user-defined in the framework input. While it is possible to extract these from the HAWC2 input, allowing the user to control these settings directly from the framework provides greater flexibility.

Input
The aerodynamic model is designed to incorporate the displacements from the structural code to account for the change in geometry. However, this input is not directly available in the this model. Instead, the new blade geometry is calculated obtaining the new half-chord centre positions, which are then used to update the geometry in the aerodynamic model for the next iteration.

Output
After running the model, plenty of aerodynamic performance information about the wind turbine rotor can be obtained. The most relevant are the force and moment distributions along the blade, which serve as inputs for the structural model. In BEVC, these values are provided at the half-chord centre in the blade's root frame of reference. Other values of interest include the power and thrust output, which are used to assess the overall performance of the rotor, and the angle of attack along the blades, which helps to better understand the loads.

2.2.2 The structural model: CoRot

The structural model used in this project employs the corotational formulation, hence the name CoRot [10], to achieve greater accuracy for large deflections in the blades compared to similar models. It adopts a multibody approach with multiple linear beams, enabling the capture of nonlinearities that are otherwise lost in the linearization of the beams.

Initialization
The model needs to be initialized with the structural data that includes the rotor geometry, the mass distribution and the stiffness properties, see table 2.4. These parameters are given to the model through a file system greatly influenced by HAWC2 input.

Input files	Description
general_input	Json file with all the input file directories
c2_pos	Centre line definition in the blade's root frame of reference
st_properties	Structural properties file
boundary	Boundary conditions
static_load	Nodal load file
static_load_distributed	Linear varying distributed load file
static_load_segment	Linear varying distributed load over a segment file

Table 2.5: Input files for the structural model code. It contains the model's parameters and inputs.

To describe the blade, there are three files that are needed (see table 2.5): the half-chord centre line file, *c2_pos*; the structural properties file, *st_properties*, and the boundary file that just specifies the node that is fixed, normally the first one. The specific format of each file is given in the code documentation [10].

For the initialization the structure loading is set to zero. Its definition is specified in the next section.

Input
The structural code takes as input the external loads, which are the aerodynamic loads and the inertial loads, and it calculates the static deflection of the blades. This is done to one blade and the solution is applied to all of them.

The loads can be applied to the nodes, distribute them in the elements or apply them in certain segments. For each of these cases there is a file that contains the loads along the blade for the six degrees of freedom: three linear forces and three moments are defined in each node. These loads are placed in the elastic centre of the blade, which in this section are called nodes, and they are defined in the blade's root frame of reference.

Output
This structural model calculates the static displacements of the blades for the given loading. The final location of the elastic centres is given in the blade's root frame of reference. This can be used to calculate the next iteration half-chord centre line and update the geometry of the aerodynamic model.

Other values of interest can be obtained, such as the reaction forces in the blade's root. However, this are not used in this project's implementation.

2.2.3 The inertial model

Since the structural model assumes that the blade's root is an inertial frame of reference, the rotational effects are not properly captured. A simple model was implemented in this project's coupling as a practical way of correcting the structural model.

The structural model solves the equilibrium equation:

$$\mathbf{K} \cdot \mathbf{d} = \mathbf{f}_{\text{ext}} \tag{2.1}$$

where $\mathbf{K}$ is the stiffness matrix, $\mathbf{d}$ is the nodal displacement and $\mathbf{f}_{\text{ext}}$ is the nodal external load vector.

This equation is calculating the steady-state deflection of the structure, since it is imposing that $\dot{d} = \ddot{d} = 0$.

But since the blade is fixed to a rotating frame of reference, the nodes experience an absolute acceleration and the equilibrium equation can be rewritten as:

$$\mathbf{M} \cdot \mathbf{a} + \mathbf{K} \cdot \mathbf{d} = \mathbf{f}_{\text{aero}} \tag{2.2}$$

where **a** is the absolute acceleration vector and **M** is the mass matrix of the blade.

The equation 2.2 can be reorder to be the same as equation 2.1.

$$\mathbf{K} \cdot \mathbf{d} = \underbrace{\mathbf{f}_{\text{aero}} - \mathbf{M} \cdot \mathbf{a}}_{\mathbf{f}_{\text{ext}}} \tag{2.3}$$

Thus, the only change that it is needed is to subtract to the aerodynamic loads the inertial loads, before using the structural model to get the deflections.

To make things easier, the structural code has an internal mass matrix, **M**, that it is used in this inertial model to calculate the loads. This matrix takes the absolute acceleration of the degrees of freedom, $\mathbf{a}^*$, in the centres of gravity and gives the inertial loads in the nodes. All of this using the rotor frame of reference, R, described in section 2.1.1.

Kinematics of the blade

Let's first understand the kinematics to obtain the absolute acceleration in the rotor frame of reference of the centres of gravity, $\mathbf{a}^*$.

Each of the nodes has six degrees of freedom: three translations and three rotations. The position vectors of a single node, $\mathbf{r}^*$, is defined as

$$\mathbf{r}^* = \begin{pmatrix} \mathbf{r} \\ \boldsymbol{\theta} \end{pmatrix} \tag{2.4}$$

where **r** is the translation vector and $\boldsymbol{\theta}$ the rotation vector. The notation * indicates that the vector includes both transnational and rotational degrees of freedom.

These vectors can be differentiated in time to get the linear acceleration, **a** , and the angular acceleration, $\dot{\boldsymbol{\omega}}$:

$$\mathbf{a}^* = \begin{pmatrix} \mathbf{a} \\ \dot{\boldsymbol{\omega}} \end{pmatrix} \tag{2.5}$$

Since the rotor is rotating at a constant speed around the y-axis:

$${}^R\boldsymbol{\omega} = \begin{pmatrix} 0 \\ \Omega \\ 0 \end{pmatrix} \longrightarrow \quad {}^R\dot{\boldsymbol{\omega}} = \begin{pmatrix} 0 \\ 0 \\ 0 \end{pmatrix} \tag{2.6}$$

So, in the end the only value that is needed is the linear acceleration vector of each node, **a**.

To calculate the absolute linear acceleration of the nodes, the rigid body kinematics formula can be used to calculate the absolute acceleration of a point B in the blade in the rotor frame of reference, R, from the centre of the rotor, A.

$$ {}^{R}\mathbf{a}_{B} = \cancel{{}^{R}\mathbf{a}_{A}} + \cancel{{}^{R}\dot{\omega}} \times {}^{R}\mathbf{r}_{AB} + {}^{R}\boldsymbol{\omega} \times ({}^{R}\boldsymbol{\omega} \times {}^{R}\mathbf{r}_{AB}) + 2 \cdot {}^{R}\boldsymbol{\omega} \times \underbrace{\cancel{{}^{R}\dot{\mathbf{r}}_{AB}}}_{{}^{R}\mathbf{v}_{rel}} + \underbrace{\cancel{{}^{R}\ddot{\mathbf{r}}_{AB}}}_{{}^{R}\mathbf{a}_{rel}} \tag{2.7} $$

Since the centre of the rotor is located in the axis of rotation, it experiences no linear acceleration, ${}^{R}\mathbf{a}_{A}$. Additionally, as it is the origin of the coordinate system, ${}^{R}\mathbf{r}_{AB} = {}^{R}\mathbf{r}_{B}$. Regarding the relative velocities and accelerations, they are zero because, in steady-state conditions, the relative positions do not change over time.

So in the end, only this is left:

$$ {}^{R}\mathbf{a}_{B} = {}^{R}\boldsymbol{\omega} \times ({}^{R}\boldsymbol{\omega} \times {}^{R}\mathbf{r}_{B}) \tag{2.8} $$

And using the velocity vector in equation 2.6, the acceleration is equal to:

$$ {}^{R}\mathbf{a}_{B} = \begin{pmatrix} -\Omega^2 \cdot r_x & 0 & -\Omega^2 \cdot r_z \end{pmatrix}^T \tag{2.9} $$

Finally, the complete acceleration vector for a given node i in the blade is:

$$ {}^{R}\mathbf{a}_{i}^{*} = \begin{pmatrix} -\Omega^2 \cdot r_{x,i} \\ 0 \\ -\Omega^2 \cdot r_{z,i} \\ 0 \\ 0 \\ 0 \end{pmatrix} \tag{2.10} $$

Inertial load

The mass matrix , **M**, in the structural code gets the absolute acceleration of the centres of mass in the rotor coordinate system, ${}^{BR}\mathbf{a}_{CG}$, and gives the resulting inertial force distribution in the elastic centre in the rotor coordinate system.

$$ {}^{R}\mathbf{f}^{*}_{\text{inertial}} = \mathbf{M} \cdot {}^{BR}\mathbf{a}^{*}_{CG} \tag{2.11} $$

where **f*** has the linear forces and the moments in this way:

$$ \mathbf{f}^{*} = \begin{pmatrix} f_x & f_y & f_z & M_x & M_y & M_z \end{pmatrix}^T \tag{2.12} $$

2.3 The coupling algorithm

The two models can independently reach a solution for the state of the wind turbine. However, as illustrated in Figure 2.4, the input and output of each model are interdependent, forming a loop. This interdependence means that solving the equations for one model requires simultaneously solving the equations for the other. Therefore, a coupling algorithm must be employed to iteratively solve the coupled system.

This problem involves a weak coupling, as each of the different physical models is solved separately and a coupling condition must be satisfied by transferring data between the different models.

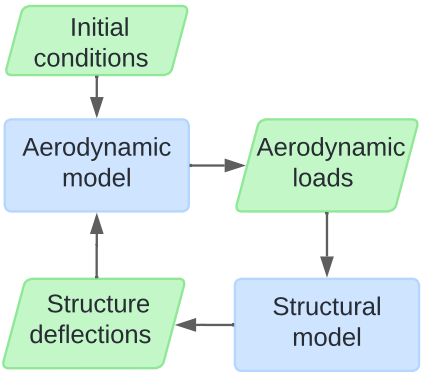

Figure 2.4: The aerodynamic and structural models are coupled since their solutions are linked to one another.

To understand this more mathematically, the following functions are defined: f_1 and f_2. The function $f_1 : X \to Y$, which is the aerodynamic model, maps the structure deflections $x \in X$ to the aerodynamic loads $y \in Y$. Conversely, the function $f_1 : Y \to X$, which is the structural model, maps the aerodynamic loads $y \in Y$ back to the structure deflections $x \in X$.

The interplay between the two models can be encapsulated in a composite function $F : X \to X$, define as $F(x) = f_2(f_1(x))$. This composite function F represents the closed-loop behaviour of the aeroelastic system, where the output of the aerodynamic model serves as the input of the structural model and vice versa.

The solution to the aeroelastic coupling system problem is characterised by finding a fixed point of the closed-loop function F. Mathematically, a fixed point $r \in X$ is defined by the equation $F(r) = r$. This implies that the deflections r, when subject to the aerodynamic model f_1, yields aerodynamic loads, that, when evaluated by the structural model f_2, return the same deflections r [14].

Identifying this fixed point is crucial, as it represents the equilibrium state of the aeroelastic system where the aerodynamic and the structural responses are in balance.

The coupling method

The method used to solve the coupling is the fixed point iteration method, which is widely used for its simplicity and effectiveness. This method evaluates the models iteratively using the state from the previous iteration:

$$x_{n+1} = F(x_n) \quad \text{until} \quad \|F(x_n) - x_{n+1}\| < \varepsilon \tag{2.13}$$

where F is a function representing the close-loop, x is the state of the system for a given iteration and ε is the residual threshold. It is called fixed point because the desired point r is a fixed point of the function $F(x)$, i.e. $F(r) \to r$ [15].

This method can be applied as if the models were black boxes, requiring no knowledge of the model derivatives or additional information [16].

Fixed point iteration methods are often prone to instability and divergence, particularly when large steps are taken in the iterations. To mitigate this issue, a relaxation factor is commonly employed. This factor slows down the convergence but enhances the robustness of the coupler, ensuring that the model reaches a solution more reliably. The modified formulation incorporating the relaxation factor, $\alpha \in (0, 1]$, is expressed as:

$$x_{n+1} = \alpha\, F(x_n) + (1 - \alpha)\, x_n \tag{2.14}$$

Typically, fixed point iteration algorithms exhibit linear convergence. However, as the relaxation factor decreases, the rate of convergence decreases, i.e. the convergence slows down.

In this project, the relaxation factor was not implemented, as none of the study case simulations indicated signs of divergence.

The coupling sequence

The coupling sequence for this particular implementation is illustrated in the flow chart in figure 2.5. It shows the different steps taken, their order and the data communicated between models.

The model is first initialized with initial conditions and then enters the iteration loop. To exit this loop, the convergence criterion must be satisfied. Inside the loop, it first calculates the loads and then the deflections. The aerodynamic and inertial loads are calculated sequentially, but since they do not depend on each other, they are shown to be in parallel in the diagram.

Instead of using the entire state vector x as shown in equation 2.13, the convergence criterion of this implementation uses only the deflections of the node in the tip. So in the end the coupling criterion is:

$$\frac{\|\vec{u}_{\text{tip,new}} - \vec{u}_{\text{tip,pre}}\|}{\|\vec{u}_{\text{tip,pre}}\|} < \varepsilon \tag{2.15}$$

where $\vec{u}_{\text{tip,new}}$ is the deflection of the tip in the last iteration, $\vec{u}_{\text{tip,pre}}$ is the deflection in the previous iteration, $\|\cdot\|$ indicates the square norm of the vectors and ε is the convergence threshold.

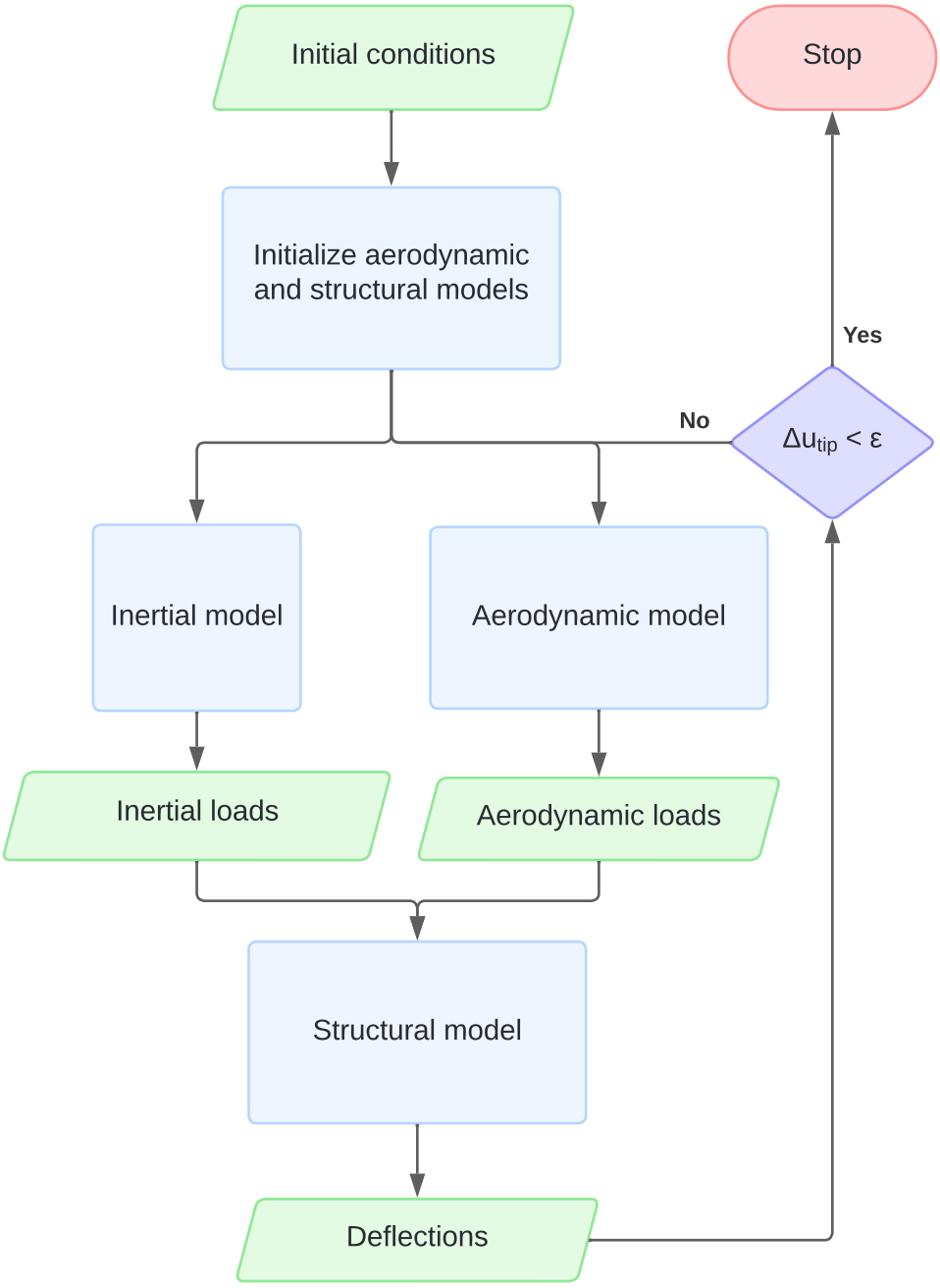

Figure 2.5: Flow chart of the coupling algorithm. Rectangles are processes, rhomboids are the inputs and outputs, and the rhombus is a decision.

2.4 The framework

In this project a modular framework was envisioned to enhance the flexibility and modularity of the coupling process allowing for more adaptable and maintainable code. To achieve this, a series of abstractions were established to minimize dependencies among different components of the code.

In computer science, a framework can be described as a reusable design of a system, typically represented by a set of abstract classes and the way in which their instances interact. This concept is crucial as it allows developers to build software systems efficiently by provide a predefined structure that can be customized for specific needs.

As previously mentioned in section 1.2, modular frameworks are used to glue together the different modules that comprise the aeroelastic model of wind turbines. This framework will compartmentalize the different modules from the coupling process.

The coupling framework consists of a series of building blocks of code. The key components are:

- Driver code: Controls the global coupling process, including the rest of components of the framework.
- Communication Code: Handles data storage and data transfer between the different components.
- Modules: Tailored code designed to handle the specific models. They are responsible for initializing, updating and running the models.

The structure of this framework is shown in the class diagram in figure 2.6 using the Unified Modeling Language (UML). This is a language used to model software systems and ease documentation of software. Each of the classes have a different purpose.

Modules

The modules are the classes that interface between the framework and the different models, specifically BEVC and CoRot in this project. Their purpose is to perform three key actions:

- *Initializing* the models with their proper input.
- *Updating* the model input during each iteration of the coupling process. For instance, the aerodynamic model must update the position of the nodes each iteration.
- Finally, *getting the results* from the model and return it in a specific format.

Each module has to be tailored to the specific model being added to the coupling. The framework in this project needs both an aerodynamic and a structural class to be defined, since they are used in the driver code.

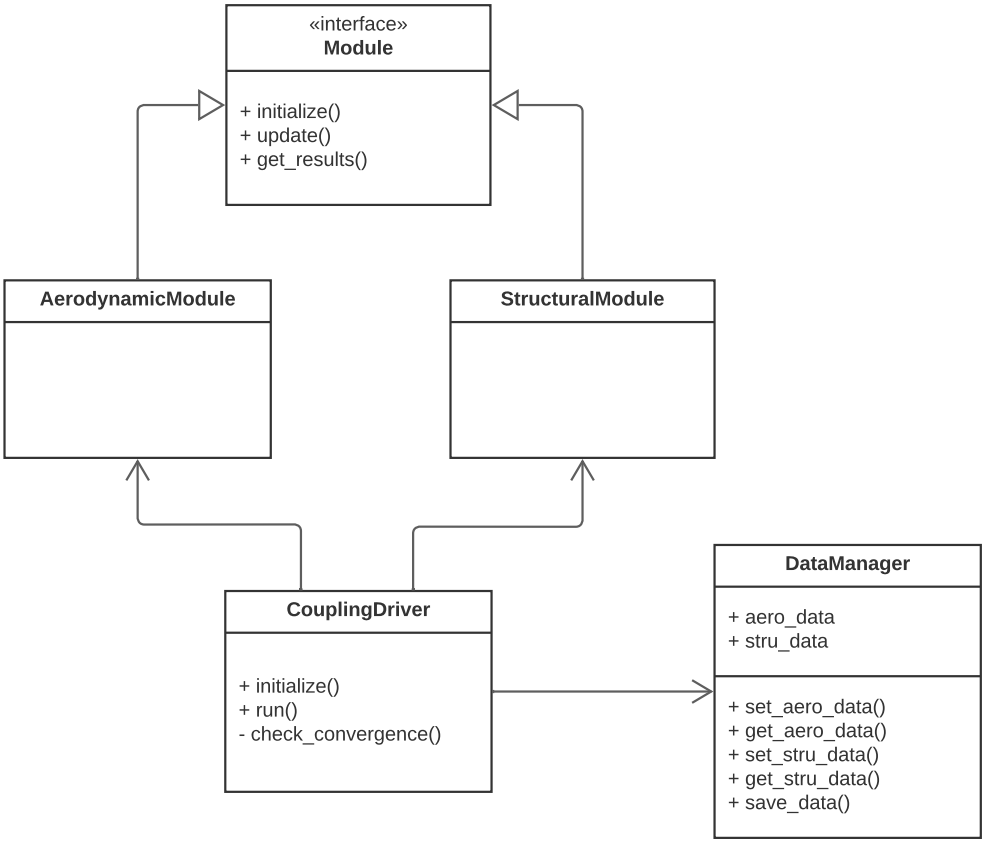

Figure 2.6: Class diagram of the coupling framework.

Data manager

The data manager handles the storage and communication of data between models. In this project, the data manager is a simple object that handles the data of each model separately.

Coupling driver

The purpose of this class is to control the overall coupling process and coordinate all components of the framework. The coupling process, as depicted in the flow chart in figure 2.5, is divided into three primary methods:

- Initialize(): This method sets the initial conditions for the wind turbine and initializes the modules.
- Run(): This method executes the coupling loop until the convergence condition is met or the maximum number of iterations is reached.

- isCoupled(): This private method checks the convergence in each iteration.

3 Verification of the implementation

In this chapter, the implemented steady-state wind turbine model is going to undergo a validation of its loads and deflections, as well as a characterization of the model's coupling convergence. The chapter is organized into three main sections: a brief introduction to the reference wind turbine, the validation and the convergence study.

The validation section focuses on comparing the model's results against those from the HAWC2 tool to assess its accuracy and reliability under various operational conditions. This ensures that the developed model can accurately replicate the behavior of a wind turbine as predicted by a well-established model.

The convergence study examines the model's behavior across different blade discretization levels to determine its rate of convergence and the optimal level discretization level of the blades.

3.1 The reference wind turbine

The wind turbine model employed for the validation and the different case studies is the 15 MW reference wind turbine developed by the International Energy Agency (IEA) [17], which brings together the efforts of researchers from the National Renewable Energy Laboratory (NREL), the Technical University of Denmark (DTU) and the University of Maine (UMaine). This reference wind turbine, depicted in 3.1, is widely utilized for benchmarking aeroelastic tools, new technologies, and design methodologies.

This model represents an offshore wind turbine with a rated power of 15 MW and a rotor diameter of 240 meters. The main design parameters of the wind turbine are summarized in 3.1. Nevertheless, it is important to note that the modelled part in the developed model only encompasses the rotor, with other components, such as the nacelle, tower, and foundation, being treated as rigid. Furthermore, the tilt angle and the cone angles are removed to simplify the geometry of the wind turbine. Lastly, due to some limitations in the structural code implementation, the offset of the centre of elasticity with respects to the half-chord centre could not be accounted for.

3.2 Validation

In this section a validation of the results of the developed model is carried out, comparing these against the results in HAWC2. The purpose of the validation is to assess the accuracy and reliability of the developed model under various operational conditions. This comparison helps ensure that the model can accurately replicate the behavior of a wind turbine, as predicted by HAWC2, a well-established tool in the industry.

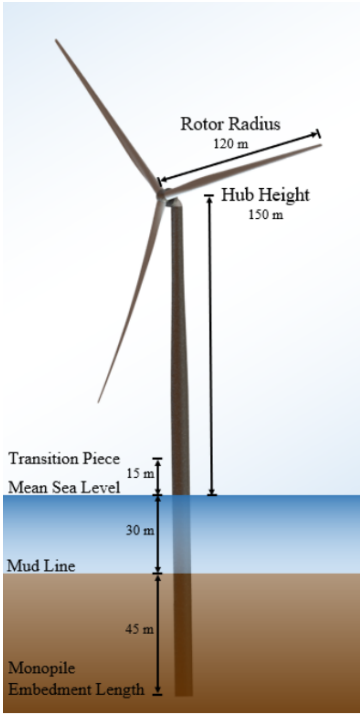

Figure 3.1: Illustration of the IEA 15 MW reference wind turbine used for the validation and different case studies [17].

3.2.1 Methodology

Setting up HAWC2

HAWC2 is a time-marching model of a wind turbine that not only models the rotor, but the entire structure up to the foundation. To make it comparable to the model developed in this project, several configurations need to be set within HAWC2.

First, all bodies of the structure, except the blades, are defined rigid. This simplifies the model and makes the results only dependent on the blades dynamics, which are the only ones modeled in the project's model. Gravity is disable in all HAWC2 bodies, aligning with the assumptions made in the project's model. Finally, the wind is configured to be uniform and constant, which means there is no wind shear, no turbulent wind boxes and no tower shadow effects incorporated in the simulations.

The aforementioned configuration allows the model to converge to a steady-state solution in the majority of cases. The model is run for a simulation time of 200 seconds, after which the convergence is checked. In certain instances, the model was unable to converge, requiring the time step size to be reduce.

The different cases

The wind turbine is simulated under a variety of operational conditions and rigidity levels to understand better the accuracy of the model and how it compares to HAWC2. Table

Parameter	Units	Value
Power rating	MW	15
Number of blades	-	3
Rated wind speed	m/s	10.59
Design tip-speed ratio	-	9
Diameter	m	240
Airfoil series	-	FFA-W3
Hub diabeter	m	7.94
Blade prebend	m	4
Blade mass	t	65

Table 3.1: Key parameters of the IEA 15 MW reference wind turbine

Case	Rigidity	Pitch [deg]	TSR [-]	U_0 [m/s]
1.1	Stiff	0	9.0	8
1.2	Torsional stiff	0	9.0	8
1.3	Fully flexible	0	9.0	8
2.1	Stiff	2	9.0	8
2.2	Torsional stiff	2	9.0	8
2.3	Fully flexible	2	9.0	8
3.1	Stiff	0	11.9	6
3.2	Torsional stiff	0	11.9	6
3.3	Fully flexible	0	11.9	6
4.1	Stiff	0	6.0	12
4.2	Torsional stiff	0	6.0	12
4.3	Fully flexible	0	6.0	12

Table 3.2: Different cases studied in the validation of the model.

3.2 summarizes the 12 cases that were found to be relevant and their configuration, grouped into four main categories:

1. Optimal operational point. The pitch is zero and the tip-speed ratio (TSR) is optimal. The chosen operational point has a free wind speed of 8 m/s, which is below the rated wind speed.

2. Pitched blades. The blades are pitched by 2 degrees, while maintaining the optimal TSR.

3. High TSR. The blades are not pitched, but the TSR is increased by reducing the free wind speed to 6 m/s while keeping the rotational speed unchanged.

4. Low TSR. The blades are not pitched, but the TSR is decreased by increasing the free wind speed to 12 m/s, again maintaining the same rotational velocity.

The purpose of having different rigidity levels is to allow for a more comprehensive comparison of the two models. The following descriptions provide a deeper understanding of each rigidity level:

- Stiff cases. These cases are achieved by significantly increasing the elastic and shear modulus in the structural properties. In this scenarios, the structural model differences are not brought into play, highlighting the differences in the aerodynamic models. By keeping the structure rigid, the impact of aeroelastic coupling is reduced, making it easier to compare purely aerodynamic responses.
- Torsional stiff. In these cases only the shear modulus was increased. This is achieved increasing just the shear modulus, resulting in blades that can bend but not twist under loads. This set up aims to minimize the coupling between bending and torsion, simplifying the coupling efforts. The blades' geometric angles do not change as dramatically due to the reduce twisting, thus affecting the aerodynamic forces to a lesser extent.
- Fully flexible. In these cases, the full coupling of both models is compared one-to-one. This level includes all the complexities of aeroelastic interactions, allowing for a comprehensive analysis of how the models perform under fully coupled conditions. The blades can both bend and twist, providing a realistic simulation of wind turbine behavior under operational conditions.

3.2.2 Case 1: optimal operational point

In this cases of the validation, the wind turbine is going to be operated at its optimal operational point for a wind speed below rated of 8 m/s. This means that the power coefficient, C_P, is maximum.

	Power			**Thrust**		
	HAWC2	Our resuts	Relative Difference	HAWC2	Our resuts	Relative Difference
Stiff	7181	7178	-0.042%	1453	1458	0.344%
Torsional stiff	7148	7120	-0.392%	1462	1468	0.410%
Flexible	6843	6902	0.862%	1304	1314	0.767%

Table 3.3: Resulting steady state power in kW and thrust in kN for case 1, optimal operational point.

Case 1.1. Rigid blades

Figure 3.2a shows the node positions along the blade span, indicating the standstill blade shape, since it is rigid. The critical information is in figures 3.2b and 3.2c, which display the force and moment distributions along the blade, respectively. Both the HAWC2 model and our model show perfect agreement in both magnitude and shape of the loads.

Table 3.3 presents the resulting steady-state power and thrust values. The differences between the models is minimal, below half a percentage point. This close match demonstrates the accuracy of the aerodynamic model under this conditions.

Case 1.2. Torsional stiff blades

The next validation step involves the torsional stiff blades. The displacements of the nodes, see figure 3.2a, show that both models predict similar final positions in steady-state.

Regarding the loads, see figures 3.2b and 3.2c, there are slight differences in the linear forces in the x-axis near the root and the moments around the y-axis close to the tip, the overall agreement is excellent.

The overall discrepancies do not significantly impact the performance predictions, with the difference in power and thrust remaining below 0.5%, see table 3.3.

Case: 1.3. Fully flexible blades

Finally, for the fully flexible blades, both models continue to demonstrate good agreement in terms of displacements, as evidenced by figure 3.2a. This consistency in predicting the blade's structural response under fully flexible conditions of the highlights the accuracy of the coupling.

This time, however, the are notable differences in the load predictions, especially in the aerodynamic forces in the axial direction and moments around the y-axis, where our model predicts slightly higher loads. Despite these differences, the overall performance of the rotor, in terms of power and thrust, remains very similar between the two models, within 1% difference, see table 3.3.

3.2.3 Case 2: pitched blades

In this section, the performance of the wind turbine with pitched blades by 2 degrees while maintaining the optimal tip-speed ratio is analyzed. This scenario helps to understand the effect of pitching in the accuracy of the coupled model.

	Power			**Thrust**		
	HAWC2	Our resuts	Relative Difference	HAWC2	Our resuts	Relative Difference
Stiff	6786	6868	1.208%	1258	1268	0.795%
Torsional stiff	6792	6870	1.142%	1270	1282	0.964%
Flexible	6286	6369	1.317%	1118	1129	0.962%

Table 3.4: Resulting steady state power in kW and thrust in kN for case 2, pitched blades by 2 degrees.

Case 2.1. Rigid blades

Figures 3.3b and 3.3c illustrating force and moment distributions along the blade indicate that both HAWC2 and our model align closely in results.

The steady-state power and thrust values presented in table 3.4 show a decrease in the agreement of the models, getting the error to be around 1%. This shows a difference in the aerodynamic models results in this configuration.

Case 2.2. Torsional stiff blades

With flexible blades without torsion, displacements are now visible, as the blades can bend under aerodynamic and inertial loads. The node positions along the blade show

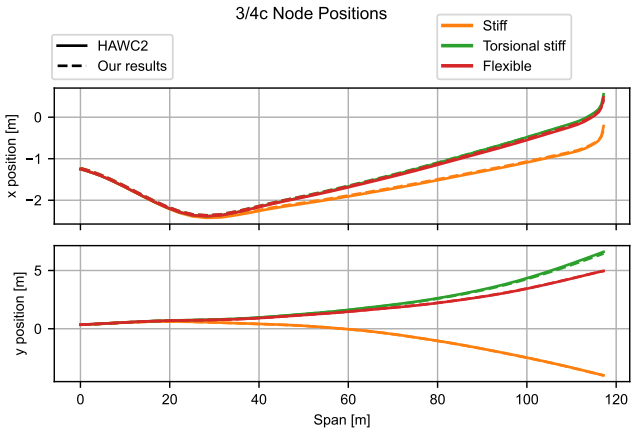

(a)

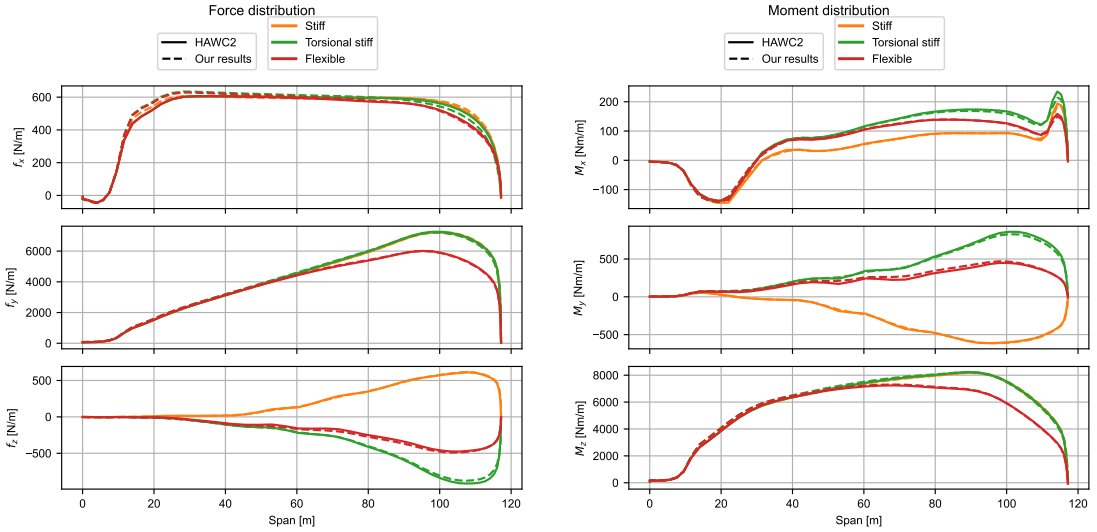

(b) (c)

Figure 3.2: For case 1, optimal operational point; positions and loads on the nodes along the span of the blade for both HAWC2 and our results, and the three different rigidities. (a) is the 3/4 chord node positions, (b) is the force distribution and (c) is the moment distribution.

similar displacements in both models, see figure 3.3a.

The aerodynamic loads, figures 3.3b and 3.3c, only have slight differences in the linear force in the x-axis, which will affect the power.

As seen in table 3.4, the overall performance is inferior to the one observed in Case 1, yet it remains around 1% of difference. The discrepancy in the tangential loads of the rotor represents the most significant contributor to the observed power difference.

Case 2.3. Fully flexible blades

In the fully flexible configuration, both models continue to show good agreement in the displacement, as evidenced by figure 3.3a. This, again, indicates that our coupling model accuratelly captures the structural and aerodynamic dynamics of the flexible blades.

However, as with previous cases, there are notable differences in the load predictions, particularly in the aerodynamic forces in the axial direction and moments around the y-axis. Our model tends to predict slightly higher loads compared to HAWC2.

Despite these differences in load predictions, the overall rotor performance, in terms of power and thrust, remains very similar between the two models. The relative differences in power and thrust are within 1.5%, as shown in table 3.4, demonstrating that the models provide closely matched performance predictions even under fully flexible conditions.

3.2.4 Case 3: high TSR

In this section, the performance of the wind turbine with a high tip-speed ratio (TSR) of 12. This is achieved maintaining the rotational speed and decreasing the free wind speed to 6 m/s. This scenario helps understand the behaviour of the coupling model in a different operational point.

	Power			**Thrust**		
	HAWC2	Our resuts	Relative Difference	HAWC2	Our resuts	Relative Difference
Stiff	2852	2548	-10.649%	1055	1026	-2.769%
Torsional stiff	2708	2488	-8.136%	1057	1036	-1.981%
Flexible	2811	2781	-1.068%	922	919	-0.323%

Table 3.5: Resulting steady state power and thrust for case 3, high TSR.

Case 3.1. Rigid blades

As in previous cases, the node position along the blade span is not of interest since the blade is rigid. In this scenario, the linear loads in figure 3.4b show significant discrepancies, especially the tangential loads along the x-axis, which are much lower than those predicted by HAWC2. Similarly, the moments are smaller in the project's model.

This results in poor performance for stiff blades under these conditions, with an underestimation of the power output of 10.6%.

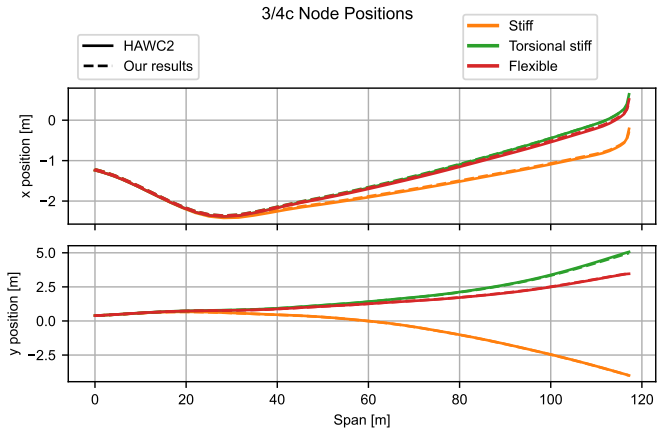

(a)

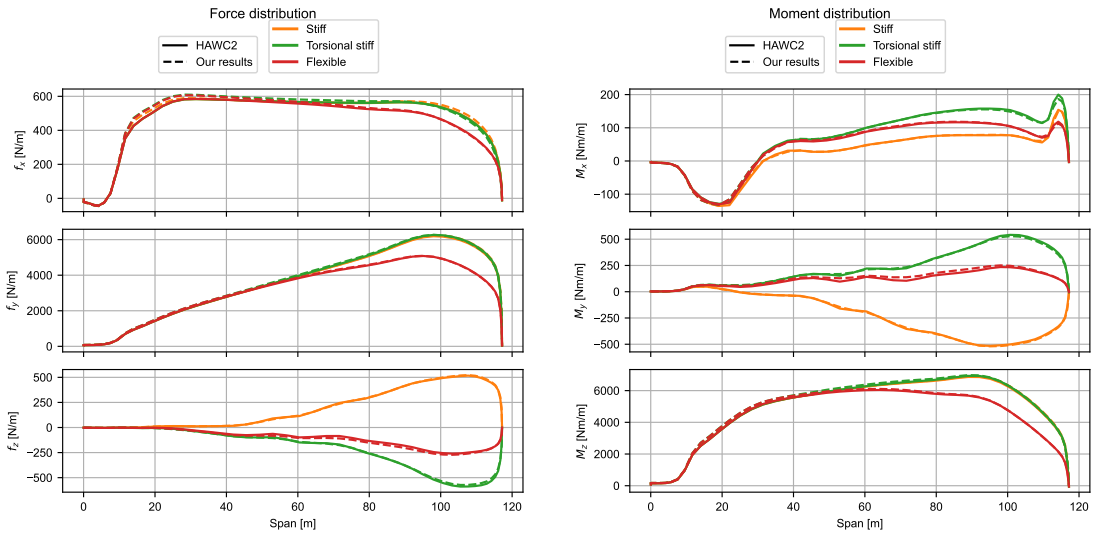

(b) (c)

Figure 3.3: For case 2, pitched blades; positions and loads on the nodes along the span of the blade for both HAWC2 and our results, and the three different rigidities. (a) is the 3/4 chord node positions, (b) is the force distribution and (c) is the moment distribution.

Case 3.2. Torsional stiff blades

When the blades are only stiff in torsion, the blades bend, resulting in inaccurate results like in the previous case, see figure 3.4a. The discrepancies in the loads (figures 3.4b and 3.2c) are still present. Only this time they have decreased..

This is reflected in the performance of the rotor, which shows an 8% lower power output and 2% lower thrust. Overall, the inclusion of bending improves the agreement between the two models.

Case 3.3. Fully flexible blades

Including torsion changes the behavior of the blade, leading to much better alignment of the loads (figures 3.4b and 3.4c). There is a notable improvement in the tangential loads and the moments generated in the airfoil.

Consequently, in this configuration, the rotor shows only 1% difference in power and less than half a percent difference in thrust compared to HAWC2.

3.2.5 Case 4: low TSR

In this section, the performance of the wind turbine with a low tip-speed ratio (TSR) of 6. This is achieved maintaining the rotational speed and increasing the free wind speed to 12 m/s. This scenario helps understand the behaviour of the coupling model in a different operational point.

Power				**Thrust**		
	HAWC2	Our resuts	Relative Difference	HAWC2	Our resuts	Relative Difference
Stiff	18728	18904	0.939%	2089	2103	0.666%
Torsional stiff	18546	18647	0.547%	2079	2089	0.460%
Flexible	17471	17548	0.441%	1900	1909	0.474%

Table 3.6: Resulting steady state power and thrust for case 4, low TSR.

Case 4.1. Rigid blades

For the scenario with rigid blades, the load distributions agree with the HAWC2 results, as illustrated in figures 3.5b and 3.5c. This agreement indicates good performance of the model in predicting aerodynamic and structural loads. The rotor performance metrics show a relative difference below 1%, further validating the accuracy of the model.

Case 4.2. Torsion stiff blades

When bending is introduced in the analysis, the resulting node positions remain very close to the ones calculated by HAWC2. The loads also show a high degree of accuracy, reflected in a power output difference of 0.55%.

Case 4.3. Fully flexible blades

Incorporating both bending and torsion, this scenario shows accurate simulations of deflections with close agreement to HAWC2. The deflections and resulting loads are precisely captured, with the only notable difference being a slight overestimation of the moments around the y-axis.

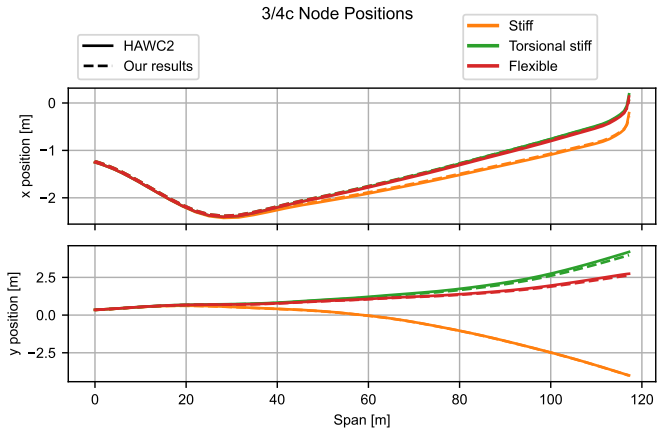

(a)

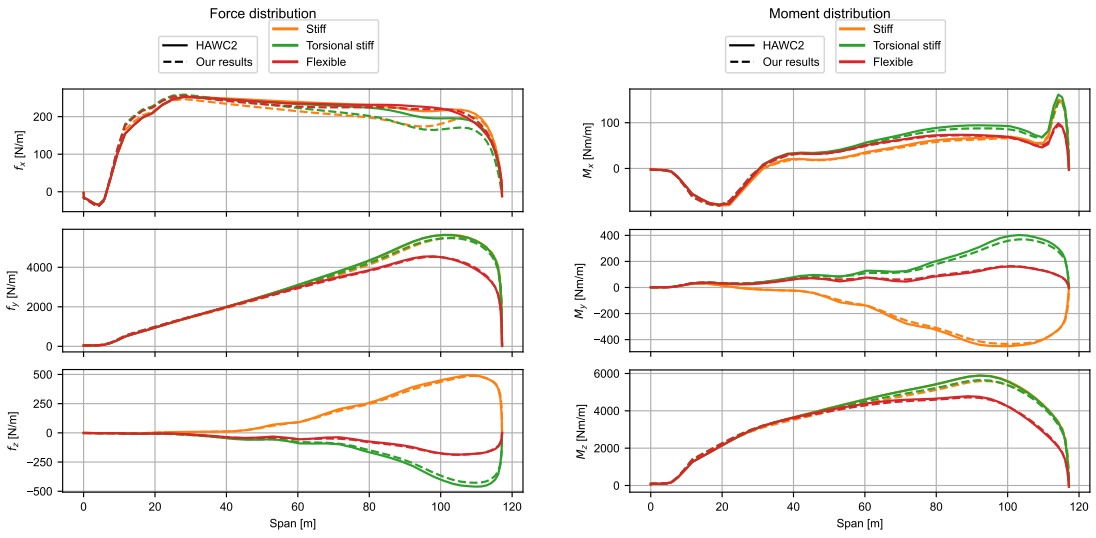

(b) (c)

Figure 3.4: For case 3, high TSR; positions and loads on the nodes along the span of the blade for both HAWC2 and our results, and the three different rigidities. (a) is the 3/4 chord node positions, (b) is the force distribution and (c) is the moment distribution.

Despite this minor discrepancies, the power and thrust performance metrics are accurate, with differences below half a percent point. This scenario proves to be the most favorable, demonstrating the model's capability to handle complex aerodynamic and structural interactions effectively.

3.2.6 Conclusion

The validation process detailed in the preceding sections has effectively demonstrated the robustness and accuracy of the developed model in simulating the behaviour of the IEA 15 MW wind turbine under various operational conditions. By comparing our results with those form the HAWC2 simulations, it has been established that our model can replicate detailed aerodynamic and structural dynamics and coupling with high fidelity.

Across different cases studies — ranging form optimal operational points to scenarios involving high and low tip-speed ratios — the developed model consistently produced results that closely align with the HAWC2 benchmarks. The discrepancies observed were minimal, typically within 1% difference for power and thrust comparisons.

3.3 Convergence study

In this case study, a convergence study is carried out to better understand the model's behaviour and to determine the optimal blade discretization for the IEA 15 MW reference wind turbine.

3.3.1 Methodology

The IEA 15 MW reference wind turbine is provided with a fixed discretization in its geometry, consisting of 34 nodes for the half-chord centre line and 30 points for the aerodynamic properties. The half-chord centre line is generated using a spline, with the other properties aligned along it.

The model is capable of discretizing the blade based on the defined spline with a varying number of nodes. Increasing the number of nodes will result in a greater number of linear beams used in the structural model, thus increasing the definition of the displacements and loads distributions outputted by the model. Similarly, the aerodynamic model will result in more detailed load distributions.

To increase the number of nodes, a cosine distribution along the span of the blade is used. This distribution places more nodes towards the tip, were gradients are higher and there is more impact on the results.

In this study, eight discretization levels are used: the first ones are coarser that the original data, with 20 and 30 nodes, representing a downgrade. The subsequent levels become finer with 40, 50, 80, 100, 150 and 200 nodes. The later serves as the benchmark case for comparing the effects of the discretization.

Regarding the model itself, it is run until convergence, meaning the solution stabilizes and does not change significantly in the subsequent iterations. The wind turbine will be operated optimally at a below-rated wind speed of 8 $\mathrm{m/s}$.

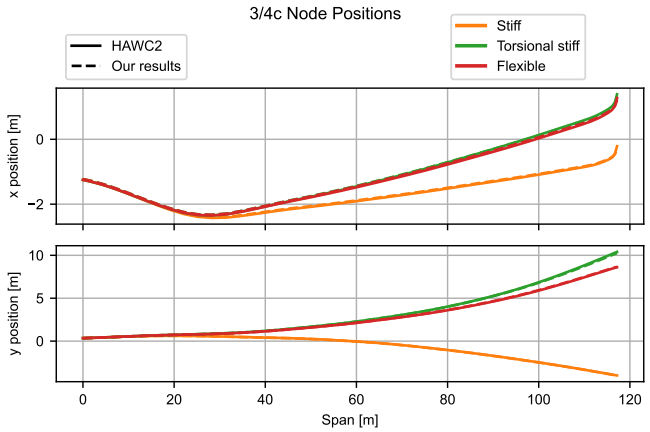

(a)

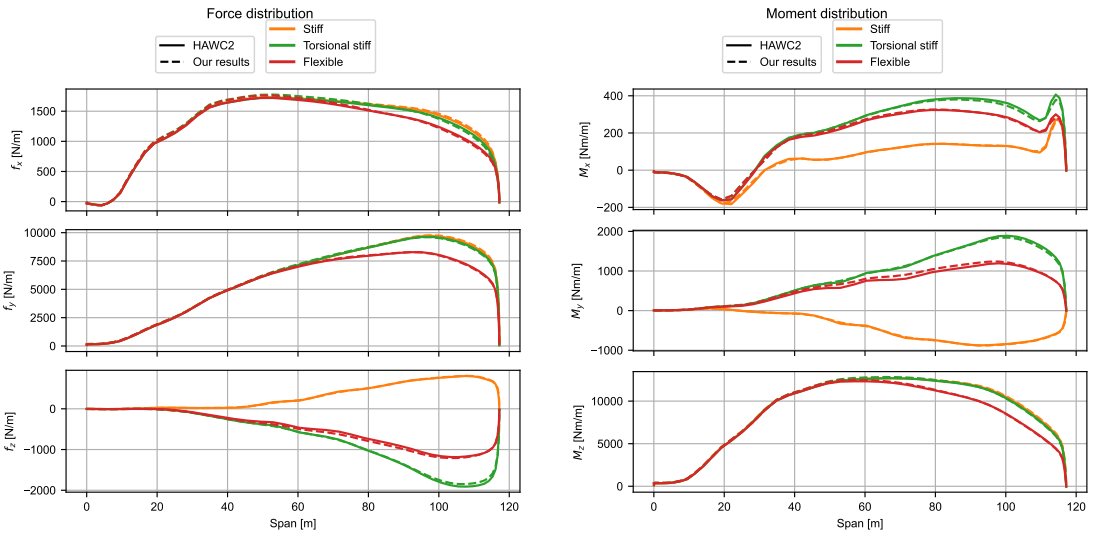

(b) (c)

Figure 3.5: For case 4, low TSR; positions and loads on the nodes along the span of the blade for both HAWC2 and our results, and the three different rigidities. (a) is the 3/4 chord node positions, (b) is the force distribution and (c) is the moment distribution.

3.3.2 Results

The convergence criterion used in this model is the change in the tip position as $\Delta u_{tip} = \|\vec{u}_{\text{tip,new}} - \vec{u}_{\text{tip,pre}}\|$, described more in detail in section 2.3, only this time it is not normalized. This value is shown in figure 3.6a for each iteration of the model in a semilogarithmic plot for each discretization level. The plot demonstrates that, across all discretization levels, the model trends towards zero in a straight line. These convergence lines exhibit different slopes, which are steeper for the cases with fewer nodes. The black lines show the slope of linear and quadratic convergence rates. Compare to them, in all case the model is close to linear or a bit slower.

Then, it is possible to determine if they converge to the same values by examining the tip deflection error, $\epsilon_{u_{\text{tip}}}$. This error is shown in figure 3.6b and it is calculated as $\epsilon_{u_{\text{tip}}}(i) = \|\vec{u}_{\text{tip},i} - \vec{u}_{\text{tip,final}}\| / \|\vec{u}_{\text{tip,final}}\|$ where $\vec{u}_{\text{tip,final}}$ is the tip deflection in the final iteration for each case. This error represents how the model converges to a final tip position at the same rate the tip deflection changes go down. In all cases we can say that all models have reach an excellent accuracy, with less than a thousandth of a percentage point of error, by the 5$^{\text{th}}$ iteration.

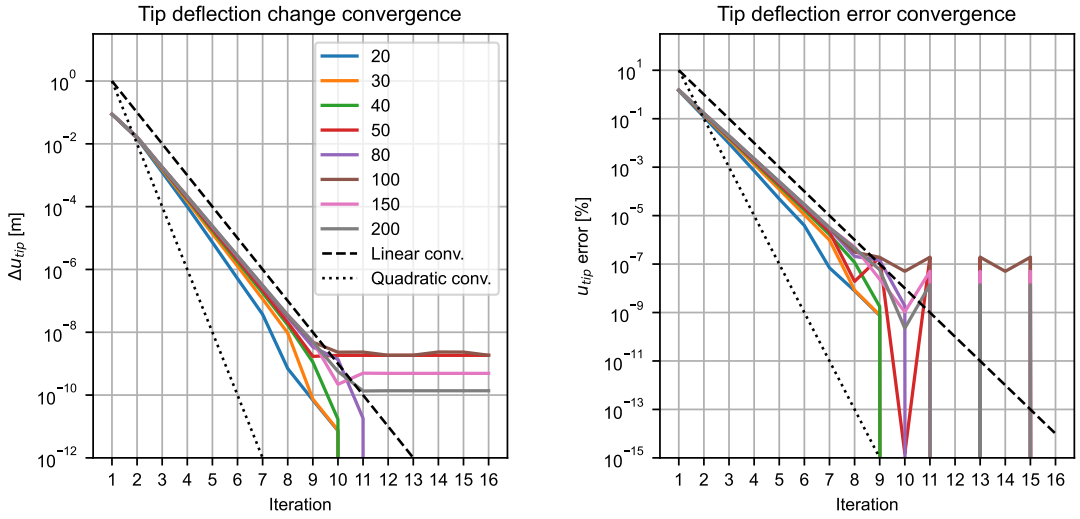

(a) (b)

Figure 3.6: Convergence study of (a) tip deflection change, Δu_{tip}, and (b) tip deflection error, $\epsilon_{u_{\text{tip}}}$, for different blade fidelities (number of nodes).

Examining the rotor performance error, specifically the power and thrust, reveals a similar pattern to the deflections, as shown in figures 3.7a and 3.7b. These figures indicate that all discretization levels converge at the same rate, close to linearly.

This convergence rate is linear as the method used to couple the models is a fix point iteration method (see section 2.3). These methods, unless accelerated with more ad-

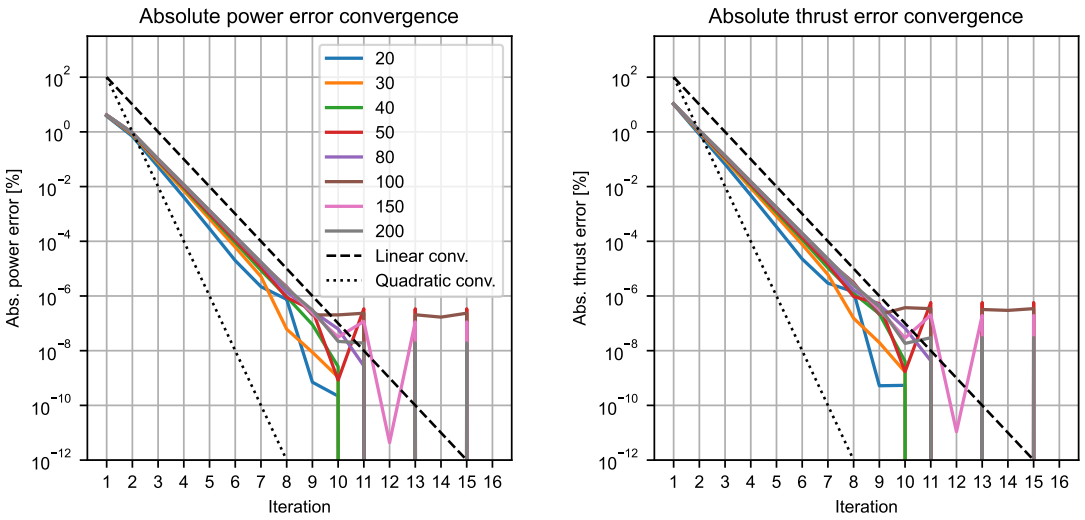

(a) (b)

Figure 3.7: Convergence study of (a) the power error, ϵ_P, and (b) the thrust error, ϵ_T, for different blade fidelities (number of nodes).

vance algorithms, exhibit linear convergence rates or slower in case of being relaxed.

The convergence rate can also be estimated using equation 3.1, which utilizes the values from four iterations: $n-2$, $n-1$, n and $n+1$. Figure 3.8 illustrates this estimation for different values of n. The estimation consistently indicates linear convergence across all discretization levels.

$$\alpha \approx \frac{\log\left(\|\vec{x}_{n+1} - \vec{x}_n\| / \|\vec{x}_n - \vec{x}_{n-1}\|\right)}{\log\left(\|\vec{x}_n - \vec{x}_{n-1}\| / \|\vec{x}_{n-1} - \vec{x}_{n-2}\|\right)} \tag{3.1}$$

It is interesting to study the level of precision achieved for the power and thrust at convergence across different discretization levels, comparing them to the highest fidelity level. In this analysis, the absolute error is defined as $\varepsilon_n = |x_n - x_{200}|/x_{200}$ where n is the number of nodes and x represent either the power or the thrust. Figure 3.9 illustrates these precision values for different node counts. It is immediately evident that both cases exhibit different convergence behaviours: while the power converges from the beginning, the thrust remains relatively unchanged in the first four discretization levels.

From this figure, it is possible to select the appropriate discretization level for a given desired precision. For regular aeroelastic simulations aimed at obtaining power and thrust curves, an error of less than 0.1% might be sufficient, suggesting the 30 nodes could be adequate for this purpose. On the other hand, there are application where

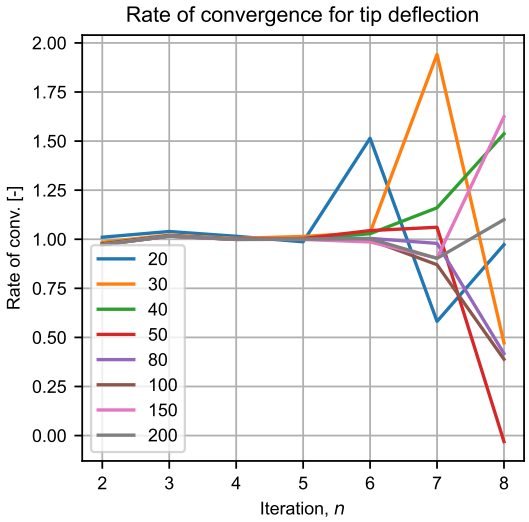

Figure 3.8: The rate of convergence for the tip deflection was estimated using Equation 3.1. This estimator indicates linear convergence across all discretization levels prior to convergence, after which it begins to fail.

higher accuracy is crucial, such as optimizing the rotor. In these cases, the optimizer needs to calculate the gradients of the wind turbine performance with respect to the design variables. For such purposes, it might be preferable to use 80 or 100 nodes ensure the necessary precision.

It is also possible to explore how this error distributes along the blade span by analysing how loads relate to power and thrust. While showing the load distribution error alone might be simpler, examining how these errors contribute to the overall rotor performance provides more insightful information. Below is a brief explanation of how these are determined.

The power generated by the rotor is the integral along the span, s, of the blade of the tangential load, f_x, multiplied by the radius, r; the rotor speed, ω, and the number of blades, N. The contribution of the aerodynamic moment, M_y, is neglected in this analysis.

$$P = N \int_0^S f_x(s) \cdot r(s) \cdot \omega \, ds + N \int_0^S \cancel{M_y(s)} \cdot \omega \, ds \tag{3.2}$$

Substituting this expression into the absolute power error formula yields:

$$\epsilon_P = \frac{|P_n - P_{\text{ref}}|}{P_{\text{ref}}} = \frac{1}{P_{\text{ref}}} \left| N \int_0^S f_{x,n}(s) \cdot r(s) \cdot \omega \, ds - N \int_0^S f_{x,\text{ref}}(s) \cdot r(s) \cdot \omega \, ds \right| \tag{3.3}$$

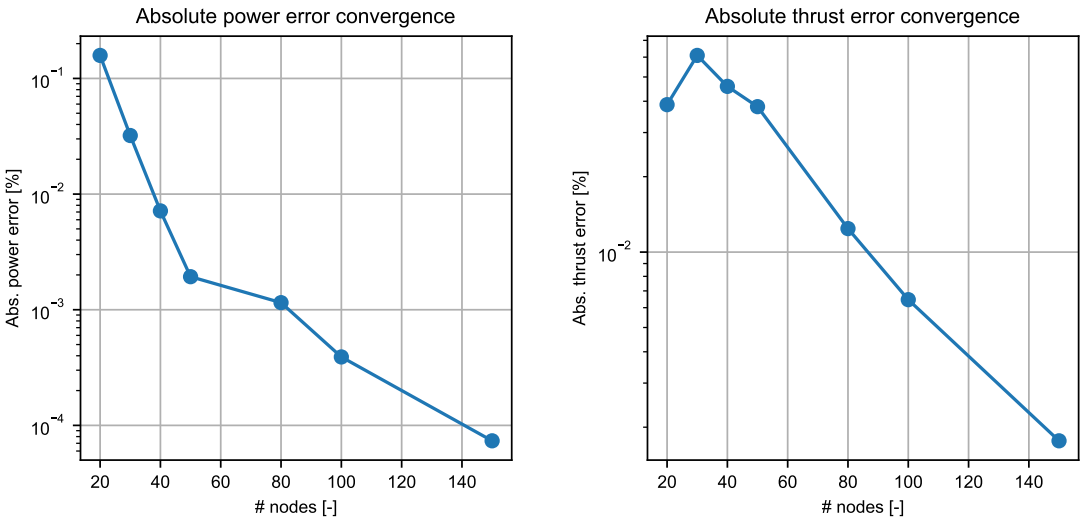

(a) (b)

Figure 3.9

where n is the number the discretization level and the reference is the case with 200 nodes.

This leads to the following expression:

$$\epsilon_P = \int_0^S \left| f_{x,n} - f_{x,\text{ref}} \right| \cdot r(s) \cdot \frac{N \cdot \omega}{P_{\text{ref}}} \, ds \tag{3.4}$$

A similar approach can be applied to the thrust, expressed as $T = N \int_0^S f_y(s) \, ds$, where f_y is the force distribution normal to the rotor plane. This yields:

$$\epsilon_T = \int_0^S \left| f_{y,n} - f_{y,\text{ref}} \right| \frac{N}{T_{\text{ref}}} \, ds \tag{3.5}$$

The integrands of these expressions, representing the distributed power error and the distributed thrust error, are plotted along the blade span in figure 3.10. It is clear that a disproportional amount of the error originates from the blade tip in all discretization levels. And surprisingly, there is a significant error contribution from the sections closer to the root.

3.3.3 Conclusion

The convergence study conducted in the IEA 15 MW reference wind turbine for the project's aeroelastic model provides valuable insights into the model's behavior and the

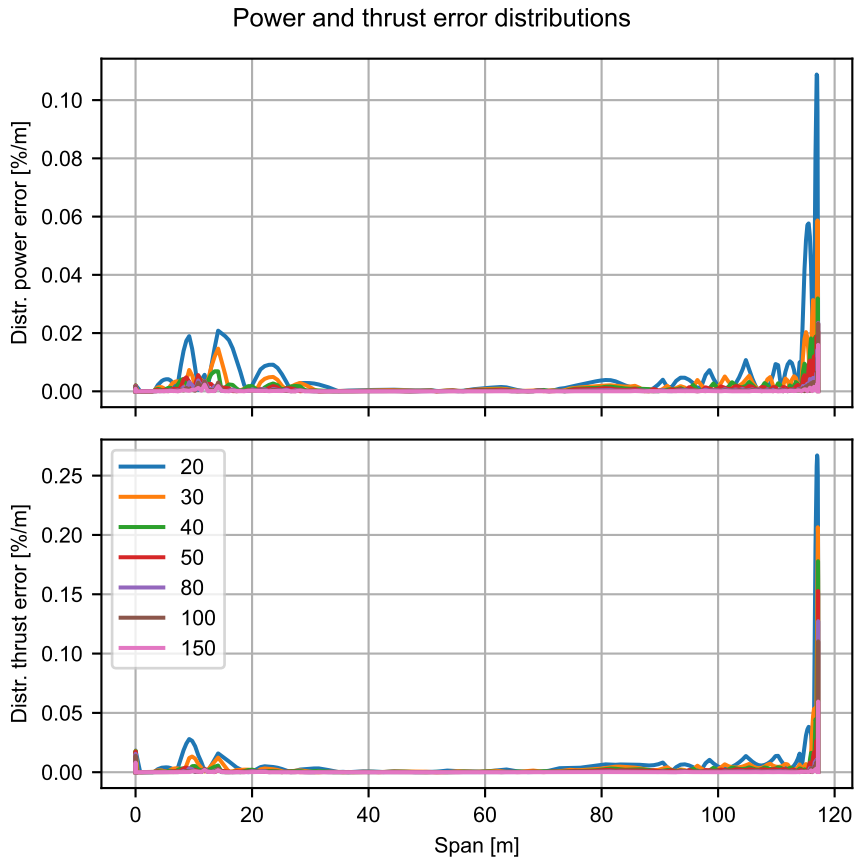

Figure 3.10: This figure shows how the power error (top) and thrust error (bottom) distribute along the span of the blade for the different fidelities in the 16th iteration. The areas around the tip and the root show the biggest differences between coarse and fine blades.

impact of blade discretization on its accuracy. The study examined various discretization levels, ranging from 20 to 200 nodes,yielding the following findings:

- *Convergence behaviour*. In all cases the model converges at a steady rate close to a linear rate of convergence, as shown in figures 3.7 and 3.6. There is a slight acceleration in convergence for the less discretized cases. Overall, the model converges very quickly, taking fewer than 10 iterations.
- *Rate of convergence*. The rate of convergence was assessed visually in the convergence plots and then estimated numerically. The estimated rate of convergence was shown to be close to one in almost all cases, except for the more less discretized cases.
- *Model precision*. After reaching convergence, the different discretization levels

exhibited varying accuracy compared to the highest fidelity case, see figure 3.9. Both curves look surprisingly different, with the power error decreasing monotonically, while the thrust error requires more nodes to decrease significantly.

- *Optimal discretization level*. It was shown that using slightly more than 30 nodes is sufficient to achieve an error below 0.1%, which is adequate for most cases. In the particularly case of optimization, where gradients evaluations are necessary, higher accuracy is required, making a discretization of 80 or 100 nodes more suitable.
- *Error distribution*. The distribution of the load errors along the blade was analyzed. In this study, they were scaled to show the power and thrust errors distributions, instead (see figure 3.10). This analysis highlighted the significant impact of the cosine distribution discretization towards the tip of the blade.

4 Conclusions

The results present in Chapter 3 demonstrate the successful development of a steady-state aeroelastic model for wind turbines. The model showed a good match of the results for different operational conditions of the wind turbine when compared to the state-of-the-art model HAWC2. Furthermore, it converges in less than ten iterations and does not require a high level of discretization to achieve accurate results, demonstrating its high performance.

4.1 Relevance

This tool has several relevant applications:

- The steady-state model is highly useful for accurately modeling wind turbine performance under a wide range of operational conditions. It also effectively calculates loads on the rotor, particularly at the blade root. These steady-state values are used to assess the design of the rotor as well as to be an input for the detail design.
- The model's results can be used to calculate the performance gradients with respect to the design variables, being able to be included in a optimizer.
- The framework allows for the integration of different structural and aerodynamic models, saving development time and offering flexibility in creating a working aeroelastic tool.

4.2 Limitations

The framework developed in this project has certain limitations and simplifications that were necessary to create a working prototype. To make it fully functional and user-friendly, several enhancements are required, including better documented code, test cases to facilitate implementation, and other basic features that other coupling frameworks have.

Regarding the steady-state results, the structural model has some limitations. Specifically, the wind turbine blade had to be simplified to neglect the elastic centre offset from the half chord centre. Addressing this issue would involve modifying the source code of the structural model to make this information accessible by the framework.

4.3 Further work

The following topics could be of interest to continue further this project:

4.3.1 Advance coupling algorithms

The coupling method used, fixed point iterations, is the first of multiple ways in which models can be coupled. This method usually converges at a linear rate, which was

confirmed in section 3.3. This approach showed robustness and fast convergence for the study cases presented in this project. However, it might be interesting to further improve this coupling in two ways:

- Incorporating *relaxation* terms and exploring the stability of the model on certain scenarios. This addition might have little to no impact in the number of iterations, but it could be essential in certain modeling scenarios.
- *Parallelizing* the structural and the aerodynamic models. Given the low number of iterations required for convergence, accelerating the coupling algorithm by increasing the rate of convergence may not be necessary. Instead, reducing the cost of each iteration by coupling the models more closely could be more beneficial. Solutions could involve coupling the models in a way that they share the residuals and converge to their respective solutions together, exchanging relevant information during a iteration.

The framework developed in this project can facilitate the implementation of these new ideas, providing a solid foundation for future iterations and improvements.

4.3.2 Coupling other models

One of the purpose of the framework is to ease the coupling of various models. Currently, it is limited to coupling structural and aerodynamic codes. It would be interesting to generalise the framework to include other types of models.

For instance, tools such as BECAS [18], a DTU tool capable of calculating cross-sectional stiffness properties from an arbitrary oriented material like fiber glass. Including BECAS could allow for the optimization of parameters related to the blade's fiber layup to improve the design of the blades.

Bibliography

[1] International Energy Agency. *Net Zero by 2050*. Licence: CC BY 4.0. Paris, 2021. URL: https://www.iea.org/reports/net-zero-by-2050.

[2] International Energy Agency. *Renewables 2021*. Licence: CC BY 4.0. Paris, 2021. URL: https://www.iea.org/reports/renewables-2021.

[3] Michael Sprague, Jason Jonkman, and Bonnie Jonkman. "FAST Modular Framework for Wind Turbine Simulation: New Algorithms and Numerical Examples". In: Jan. 2015. DOI: 10.2514/6.2015-1461.

[4] Jason Jonkman. "The new modularization framework for the FAST wind turbine CAE tool". In: *51st AIAA aerospace sciences meeting including the new horizons forum and aerospace exposition*. 2013, p. 202.

[5] J. G.Holierhoek. "5 - Aeroelastic design of wind turbine blades". In: *Advances in Wind Turbine Blade Design and Materials*. Ed. by Povl Brøndsted and Rogier P.L. Nijssen. Woodhead Publishing Series in Energy. Woodhead Publishing, 2013, pp. 151–173. ISBN: 978-0-85709-426-1. DOI: https://doi.org/10.1533/9780857097286.1.150.

[6] H. Dowell. *A Modern Course in Aeroelasticity*. Solid Mechanics and Its Applications. Springer International Publishing, 2021. ISBN: 9783030742362. URL: https://books.google.es/books?id=fppIEAAAQBAJ.

[7] Morten Hansen. "Aeroelastic Properties of Backward Swept Blades". In: Jan. 2011. ISBN: 978-1-60086-950-1. DOI: 10.2514/6.2011-260.

[8] W. Collier et al. "Aeroelastic Code Comparison Using the IEA 22MW Reference Turbine: Article No. 052042". In: *Journal of Physics: Conference Series* 2767.5 (2024). ISSN: 1742-6588. DOI: 10.1088/1742-6596/2767/5/052042.

[9] Ralph Johnson. "Frameworks = (Components + Patterns)". In: *Commun. ACM* 40 (May 1997), pp. 39–42. DOI: 10.1145/262793.262799.

[10] Ozan Gözcü, Emre Barlas, and Jens Damholt Richardt. *Corotational beam formulation*. Jan. 2023. DOI: 10.5281/zenodo.7533686. URL: https://doi.org/10.5281/zenodo.7533686.

[11] A. Li et al. "A computationally efficient engineering aerodynamic model for non-planar wind turbine rotors". In: *Wind Energy Science* 7.1 (2022), pp. 75–104. DOI: 10.5194/wes-7-75-2022. URL: https://wes.copernicus.org/articles/7/75/2022/.

[12] Lars Christian Henriksen, Carlo Tibaldi, and Leonardo Bergami. "HAWCStab2 user manual". In: *Technical report„ DtU Vindenergi (EN)* (2015).

[13] Richardt Jens Damholt. *Modelling of wind turbine blades by beam elements from complementary energy*. 2022.

[14] Jonathan R Senning. "Computing and estimating the rate of convergence". In: *Wenham: Gordon College* (2007).

[15] I Ramiere and T Helfer. "Acceleration methods for fixed point coupled problems iterations". In: *Numerical Methods in Coupled Problems 2017*. 2017.

[16] Qun Zhang and Song Cen. *Multiphysics Modeling: Numerical Methods and Engineering Applications: Tsinghua University Press Computational Mechanics Series*. Elsevier, 2015.

[17] Evan Gaertner et al. “IEA Wind TCP Task 37: Definition of the IEA 15-Megawatt Offshore Reference Wind Turbine”. In: (Mar. 2020). DOI: 10.2172/1603478. URL: https://www.osti.gov/biblio/1603478.

[18] J. P. Blasques et al. “Accuracy of an efficient framework for structural analysis of wind turbine blades”. In: *Wind Energy* 19.9 (2016), pp. 1603–1621. DOI: https://doi.org/10.1002/we.1939.

Technical
University of
Denmark

Frederiksborgvej 399
4000 Roskilde

www.wind.dtu.dk